Identification of therapeutic targets for 16 clinical diseases by integrating human plasma proteome with genome

Shifang Li, Meijiao Gong

Laboratory of Immunology and Vaccinology, FARAH, ULiège, Liège 4000, Belgium.

Correspondence:

Shifang Li, fruceslee@gmail.com

Laboratory of Immunology and Vaccinology, FARAH, ULiège, Liège 4000, Belgium

Abstract

The proteome is an abundant source of potential therapeutic targets, and a comprehensive evaluation of proteins as therapeutic targets for a wide range of diseases is required. By screening 4,907 plasma proteins, we conducted a systematically two-sample proteome-wide Mendelian randomisation (MR) study to uncover potential therapeutic targets for 16 clinical diseases. Following MR analysis and stringent process filtering, a total of 79 causative plasma proteins (false discovery rate<0.05) were discovered. Colocalization analysis (Posterior Probability H4>0.8) further supported the causality of three proteins (MAP2K1, GFRA1, and THBS3) in gastroesophageal reflux disease; LYPLAL1 in keratoconus; three proteins (PCSK9, ANGPTL4, and GCKR) in familial hyperlipidemia; CRAT in atopic eczema; three proteins (IRF3, CA12, and TNFRSF1B) in hypothyroidism; AIF1 in age-related hearing impairment; and SCARF2 in alopecia. Interestingly, having a genetically higher circulating CA12 level is associated with a lower risk of hypothyroidism (OR=0.47, *p*-value=1.68e-05, Posterior Probability=0.82). Single-cell RNA sequencing analysis showed that CA12 was mainly expressed in fibroblasts and epithelial cells in patient thyroid tissue and that its expression increased in older adults. Furthermore, with a proportion of 3.8%, hypothyroidism appears to mediate the effect of IRF3 on idiopathic pulmonary fibrosis, according to mediation analysis. Overall, our research could provide new insights into the etiology of clinical diseases as well as intriguing targets for the development of screening biomarkers and therapeutic treatments.

Introduction

Plasma proteins are involved in numerous essential physiological processes, such as immunomodulation, substance transport, signaling, and homeostasis maintenance, and their dysregulation has been frequently reported in a variety of diseases, implying that these dysregulated proteins are involved in disease pathogenesis [1-2]. Given the importance of plasma proteins in disease and the fact that plasma proteins are a primary source of therapeutic targets, identifying disease-related plasma proteins can assist in deciphering disease pathophysiology and providing possible molecular targets for drug development [3-4]. Currently, large-scale proteomics study have uncovered over 18,000 protein quantitative trait loci (pQTLs) spanning over 4,800 proteins, including over 1,800 independent *cis*-pQTLs [5]. Through Mendelian randomisation (MR), these studies provide a significant data resource for systematically understanding the causal impact of plasma proteins on clinical disease. Normally, MR employs naturally randomized genetic diversity at the moment of conception as a natural experiment to uncover the causal relationship between exposure and disease, reducing the risk of reverse causation and confounding bias [6]. Proteome-wide MR has currently revealed important insights into the etiology of stroke, idiopathic pulmonary fibrosis (IPF), and COVID-19, as well as the prioritization of therapeutic targets [7-9]. Indeed, drugs containing human genetic evidence are more likely to succeed in Phase II and Phase III trials, with human genetic data supporting two-thirds of FDA-approved drugs in 2021 [10-12].

In this study, we utilized proteome-wide MR to identify circulating protein biomarkers linked with 16 clinical traits by integrating the human plasma proteome with genetic data. Colocalization analyses are conducted to determine the robustness of the proteins' instrumental variables. Furthermore, we performed single-cell sequencing data analysis and mediation analysis to identify the enriched cell types of candidate proteins in tissues as well as the potential mechanisms mediated between diseases, respectively.

Methods

Proteomic data source

A large-scale protein quantitative trait loci (pQTL) study in 35,559 Icelanders yielded the largest and most thorough genome-wide association studies (GWAS) summary datasets on 4,907 circulating proteins [5]. The detailed description of the datasets can be found in the original study [5]. In brief, the plasma protein levels were determined using the SomaScan version 4 assay from SomaLogic, and the pQTL datasets were made up of associations between genome-wide genetic variations and plasma proteins that were adjusted for age and gender using the BOLT-LMM linear mixed model. As instrumental variables in the following MR analysis, genome-wide significant and independent single nucleotide polymorphisms (SNPs) with *p*-value<5e-08 and r^2<0.001 of pQTLs were employed.

16 clinical traits data sources

To identify the potential therapeutic targets, the GWAS summary statistics from 16 diseases, including alopecia (ID: GCST006661, 36,166 cases and 16,708 controls), gastroesophageal reflux disease (71,522 cases and 261,079 controls), keratoconus (ID: GCST90013442, 2,116 cases and 24,626 controls), selective IgA deficiency disease (ID: GCST003814, 1,635 cases and 4,852 controls), fibromuscular dysplasia (ID: GCST90026612, 1,556 cases and 7,100 controls), age-related hearing impairment (ID: GCST90012115, 125,688 cases and 205,071 controls), familial hyperlipidemia (ID: GCST90104003, 3,838 cases and 345,384 controls), atopic eczema (ID: GCST90027161, 22,474 cases and 774,187 controls), Brugada syndrome (ID: GCST90086158, 2,820 cases and 10,001 controls), cataract (ID: GCST009963, 21,679 cases and 387,283 controls), uterine fibroid (ID: GCST009158, 20,406 cases and 223,918 controls), amyotrophic lateral sclerosis (ID: GCST90027164, 27,205 cases and 110,881 controls), acne (ID: GCST90245818, 34,422 cases and 364,991 controls), posterior urethral valve (ID: GCST90134327, 756 cases and 4,823 controls), hypothyroidism (ID: GCST90204167, 51,194 cases and 443,383 controls), and unipolar depression (ID: GCST006477, 66,809 individuals) were retrieved from the GWAS Catalog (https://www.ebi.ac.uk/gwas/) when an ID was provided. To the best of our knowledge, the exposure sample dataset (4,907 proteomic data) did not overlap with the outcome (16 clinical traits). Further information on the outcome dataset is

listed in **Supplementary Table 1**. If standard error and effect size are missing but z-scores are included in the GWAS summary statistics file, effect size and standard error can be calculated as follows:

$$effect\ size = \frac{z}{\sqrt{2 * p(1-p) * (n+z^2)}}$$

$$standard\ error = \frac{1}{\sqrt{2 * p(1-p) * (n+z^2)}}$$

where n is the number of individuals used in the association study and p is the *p*-value for the association study.

Mendelian randomisation analysis

Based on the presence of non-overlapping samples between exposure (4,907 proteome data) and outcome (16 clinical traits), two-sample MR analysis has been performed using the TwoSampleMR, as previously described [13-14]. In brief, the data were harmonized after clumping (r^2<0.001) to exclude ambiguous SNPs with non-concordant alleles and palindromic SNPs. Following that, the Wald ratio method was used to generate effect estimates when considering a plasma protein instrumented by a single SNP, and the fixed-effect Inverse Variance Weighted (IVW) method was employed for proteins instrumented by two or more SNPs, followed by heterogeneity analysis. To test the consistency of the associations, additional methods such as simple mode, weighted mode, weighted median, and MR-Egger were applied. The MR-Egger intercept test was used to detect probable unbalanced pleiotropy (horizontal pleiotropy). The PhenoScanner (http://www.phenoscanner.medschl.cam.ac.uk/) databases were utilized to investigate whether variants had possible pleiotropic associations with other diseases or traits when fewer than three genetic instrumental factors were employed in MR analysis. Associations with *p*-value<5e-08 were deemed significant. In a heterogeneity test, we calculated I^2 statistics with the "Isq()" function and heterogeneity *p*-value with the "mr_heterogeneity()" function; results with an I^2> 50% and a heterogeneity *p*-value (Q_pval<0.05) were considered heterogeneous (substantial heterogeneity) [8]. The F-statistic was calculated to quantify instrument strength, and an F-statistic greater

than 10 indicated an adequately powerful instrument. To account for multiple tests, the Benjamini-Hochberg correction, which governs the false discovery rate (FDR), was implemented. The association with a *p*-value of 0.05 but a Benjamini-Hochberg adjusted *p*-value greater than 0.05 was considered nominally significant, while the association with a Benjamini-Hochberg adjusted *p*-value greater than 0.05 was considered significant. Furthermore, the Steiger filtering approach was used to verify the validity of the causal direction between the hypothesized exposure and outcomes using the directionality_test() function in the "TwoSampleMR" package [14]. In addition, we performed a leave-one-out analysis to examine whether the MR estimates could be explained by a single SNP (removing estimates where all but one leave-one-out configuration had a *p*-value<0.05). Only MR results that met all of the following criteria were chosen to avoid complex causation relationships: (1) MR-Egger regression revealed no pleiotropy (*p*-value>0.05); (2) true causal direction and Steiger *p*-value<0.05; (3) heterogeneity test I^2<0.5; (4) leave-one-out analysis MR *p*-value<0.05 after removing outliers; and (5) FDR<0.05.

Colocalization Analysis

Colocalization analysis was executed to figure out whether the protein and diseases shared the same causative genetic variations and to rule out confounding owing to linkage disequilibrium (LD). This was performed using the "coloc" R package [15]. The following five mutually exclusive hypotheses were tested: (1) Neither protein nor disease has a causal SNP (H0); (2) only protein has a causal SNP (H1); (3) only disease has a causal SNP (H2); (4) both protein and disease have a causal SNP, but the two causal SNPs differ (H3); and (5) both protein and disease have a causal SNP and share the same SNP (H4). To measure the support for each hypothesis, the posterior probability was adopted. A posterior probability for H4 (PH4) of more than 80% was regarded as significant evidence of colocalization.

Single-cell RNA sequencing analysis

Single-cell RNA-sequencing of 54,762 cells taken from normal thyroid tissue from 7 individuals who had thyroidectomy and had verified instances of differentiated thyroid carcinoma were retrieved from Gene Expression Omnibus

147 (https://www.ncbi.nlm.nih.gov/geo/, GSE182416) [16]. Seurat 4.2.0 was used for
148 processing and analyzing the single-cell dataset, as previously stated [13]. In short,
149 low-quality cells by selecting feature numbers ranging from 200 to 3000 were
150 excluded. The data were normalized using the "LogNormalize" method using the
151 "NormalizeData" function. The "vst" selection method in the "FindVariableFeatures"
152 function yielded a total of 2000 highly variable genes for each sample. The
153 "FindIntegrationAnchors" function was utilized to correct the batch effect and merged
154 the 7 patients for further analysis. The k-nearest neighbors were determined using
155 principal component analysis (PCA). For data visualization, the dimension reduction
156 approach UMAP (Uniform Manifold Approximation and Projection) was utilized.
157 Cell type annotation was carried out in their study based on the specific gene
158 expression [16].

159 **Mediation analysis**

160 The product of coefficients approach was employed to quantify the impacts of
161 proteins on IPF outcomes via hypothyroidism for proteins that causally are associated
162 with IPF and hypothyroidism, as mentioned by Yoshiji and her colleagues [8]. In brief,
163 the effect of IRF3 on hyperthyroidism was first evaluated and then multiplied by the
164 effect of hyperthyroidism on IPF. Following that, the proportion of the entire effect of
165 IRF3 on IPF mediated by hyperthyroidism was calculated by dividing the
166 hyperthyroidism-mediated effect (hyperthyroidism-to-IPF) by the overall effect
167 (IRF3-to-IPF) [8,17].

168 **Results and discussion**

169 **Identification of causal proteins associated with clinical traits**

170 The MR analysis was used to evaluate the causal effects of 4,907 plasma proteins
171 on 16 diseases by using *cis*-pQTLs (pQTLs that reside within a 1 Mb region around a
172 transcription start site of a protein-coding gene) for these proteins as instrumental
173 variables and 16 clinical traits as outcomes (**Figure 1A** and **Supplemental Table 1**).
174 Given that *cis*-pQTLs are more likely than *trans*-pQTLs to directly alter the
175 transcription or translation of their linked gene, the likelihood of directional horizontal
176 pleiotropy is considerably reduced [8]. Following MR analysis and stringent process

filtering (**Method** and **Figure 1A**), a total of 79 plasma proteins were evaluated for associations with 16 clinical traits (**Figure 1B**, **Supplemental Figure 1** and **Supplemental Table 1**). Particularly, the causal associations were found for 10 clinical traits, including alopecia (6 proteins), gastroesophageal reflux disease (15 proteins), Keratoconus (3 proteins), selective IgA deficiency disease (2 proteins), age-related hearing impairment (12 proteins), familial hyperlipidemia (8 proteins), atopic eczema (4 proteins), Brugada syndrome (1 protein), amyotrophic lateral sclerosis (1 protein), and Hypothyroidism (27 proteins). For example, a genetic tendency to elevated LYPLAL1 was linked to an increased risk of keratoconus (OR per-1-SD higher plasma protein level [95% confidence interval (CI)]=2.52[1.56, 4.06]; *p*-value=0.00014). Higher levels of genetically predicted CRAT were linked to an increased incidence of atopic eczema (OR[95% CI]=1.63[1.27, 2.10]; *p*-value=0.00012). Genetically determined higher SCARF2 levels were associated with a higher risk of alopecia (OR[95%CI]: 1.23[1.11, 1.36]; *p*-value=3.91e-05). It is worth noting that the causative protein that is significantly linked to one clinical trait may also be linked to other clinical traits, while this is nominally significant (**Figure 1B**). For example, THBS3, which was associated with an increased risk of gastroesophageal reflux disease (OR[95%CI]=1.31[1.15, 1.49]; *p*-value=6.2e-05), was also linked to a higher risk of cataract (OR[95%CI]=1.014[1.003, 1.025]; *p*-value=0.0125) and uterine fibroid (OR[95%CI]=1.32[1.05, 1.67]; *p*-value=0.016). Furthermore, CRAT, which was linked to atopic eczema, was also associated with a higher risk of age-related hearing impairment (OR[95%CI]=1.079[1.022, 1.139]; *p*-value=0.0059) and fibromuscular dysplasia (OR[95%CI]=3.28[1.11,9.71]; *p*-value=0.031). These findings indicated an opportunity for existing pharmaceutical repurposing in the prevention of disease. In fact, inhibitors of interleukin-23 (IL-23) signaling, initially developed for psoriasis, have been repurposed for Crohn's disease based on GWAS that found links between genetic variants in the IL23R gene and Crohn's disease [3,18,19]. Similarly, IL-17A signaling inhibitors established for psoriasis, rheumatoid arthritis, and uveitis have been investigated and approved for ankylosing spondylitis based on GWAS findings [3]. Notably, LYPLAL1, which has

been connected to an increased risk of keratoconus, has also been linked to a lower risk of alopecia (OR[95%CI]=0.87[0.77, 0.995]; *p*-value=0.043) and atopic eczema (OR[95%CI]=0.74[0.60, 0.92]; *p*-value=0.0062). These findings suggested that when repurposing drugs, it is essential to consider the potential effects caused by multiplicity.

Colocalization analysis was then implemented to determine whether previously identified relationships between proteins and clinical traits were driven by linkage disequilibrium (LD) (**Figure 1C**). Among the 79 causative proteins, 13 showed higher colocalization evidence (posterior probability PH4>0.8), whereas two showed medium colocalization evidence (posterior probability PH4>0.7) (**Figure 1D**). For example, the colocalization indicated that the genetic variations linked to CRAT, LYPLAL1, and THBS3 (*cis*-pQTLs) were caused by the same genetic variants that underpin the association with individual clinical traits (**Figure 1E**). For the other 64 causative proteins, there was no colocalization evidence (posterior probability PH4<0.6), indicating that the MR findings for these proteins were likely biased by LD.

Genetically increased circulating CA12 level is associated with a reduced risk of hypothyroidism

Based on the MR and colocalization analysis results, the causative protein related to the clinical traits was sought to further examine the role they played. In the case of hypothyroidism, among the three causative proteins, a one standard deviation rise in genetically predicted CA12 levels was linked with a lower risk of hypothyroidism (OR=0.47, 95%CI 0.33-0.66, *p*-value=1.68e-05) (**Figure 1B, Figure 2A** and **Supplementary Tables 1**). To confirm the premise of a lack of directional pleiotropy, which can reintroduce confounding, we used PhenoScanner (http://www.phenoscanner.medschl.cam.ac.uk/) to find out whether the CA12 *cis*-pQTLs were related to any characteristics or diseases at the genome-wide significant threshold of *p*-value<5e-08. The deCODE study's primary *cis*-pQTL for CA12 (rs7183733) was linked to dentures (**Supplementary Tables 1**). Indeed, employing CA12 *cis*-pQTL as exposure and dentures as outcomes, MR analysis

revealed that CA12 levels were expected to impact dentures (OR=1.12, 95%CI 1.08-1.16, *p*-value=5.59e-12) with no reverse causation (*p*-value=1.83e-04, MR-Steiger test). This finding implies that the association between CA12 and dentures is a case of vertical pleiotropy, which does not contradict MR explanation. GTEx v8 (https://gtexportal.org/), which contains expression data from 49 tissues and 838 individuals, was used to investigate the tissues in which CA12 is expressed. When compared to whole blood, CA12 was highly expressed in numerous tissues, including the thyroid (*p*-value<0.001) (**Figure 2B**). To better understand the cell type of origin of CA12, we examined single-cell CA12 expression in human thyroid tissues from thyroidectomy patients (GSE182416, available at https://www.ncbi.nlm.nih.gov/geo/) [16]. CA12 was highly enriched in thyroid epithelial cells and fibroblasts in single-cell sequencing as compared to other cell types in adipose tissues (*p*-value<0.001) (**Figure 2C**). No difference in expression between epithelial cells and fibroblasts was found (*p*-value>0.05). These findings suggested that certain cell types may be accountable for local CA12 production in these tissues. Furthermore, we noticed that CA12 was considerably more expressed in older persons (*p*-value<0.001) (**Figure 2D**), who had a greater prevalence and incidence of hypothyroidism than young ones [20]. Taken together, these findings imply that CA12 may be an appropriate target for hypothyroidism.

In fact, the causative protein found in the study might be utilized to infer disease mediator associations [7]. As an example, recent research has shown that hypothyroidism has a positive causal effect on IPF [21]; however, the mechanisms underlying this association are not well understood. To evaluate the indirect effect of proteins on IPF outcomes via hypothyroidism, we performed a mediation analysis utilizing the effect estimates from two-step MR and the overall effect from primary MR. To accomplish this, the largest GWAS of IPF (2,668 cases and 8,591 controls) was extracted from a recent study [22] and three proteins (IRF3, CA12, and TNFRSF1B) that have a causal effect on hypothyroidism were initially used to identify a causal effect on IPF using MR analysis, as described above. Surprisingly, only IRF3 was found to have a causal effect on IPF (*p*-value<0.05/3=0.016,

Bonferroni-adjusted for three proteins) (OR=2.79, 95%CI 1.29-6.02, *p*-value=0.0088) (**Figure 2E** and **Supplementary Tables 1**). Following that, the product of coefficients method was utilized to assess the mediation effect, and 3.8% of the IRF3 mediation affect on IPF via hypothyroidism was uncovered (**Figure 2F**).

Overall, our analysis identified 13 putative causative proteins for clinical traits by integrating proteogenomics research. More research is needed to determine the viability of the 13 discovered proteins as therapeutic targets for clinical disease therapy. Furthermore, the detailed mechanism by which these proteins alter clinical traits should be explored in depth using a multi-omics approach.

Competing interests

None declared.

Contributors

SF was involved in conceptualization. SF was involved in the analysis. MJ was involved in the data collecting. SF was involved in writing, reviewing, and editing.

Acknowledgments

We would like to thank the IPF GWAS Collaborative Group for providing us with the IPF GWAS summary data. The authors would also like to thank the other researchers who contributed to developing the GWAS datasets utilized in this work for making them available for research purposes.

References

1 Henning RH & Brundel BJJM. Proteostasis in cardiac health and disease. ***Nat Rev Cardiol***. 2017;14:637-53. doi:10.1038/nrcardio.2017.89.

2 Walker KA, Chen J, Shi L, et al. Proteomics analysis of plasma from middle-aged adults identifies protein markers of dementia risk in later life. ***Sci Transl Med***. 2023, 15, eadf5681. doi:10.1126/scitranslmed.adf5681.

3 Trajanoska K, Bhérer C, Taliun D, et al. From target discovery to clinical drug development with human genetics. ***Nature***. 2023;620:737–45. doi:10.1038/s41586-023-06388-8.

4 Wallentin L, Eriksson N, Olszowka M, et al. Plasma proteins associated with cardiovascular death in patients with chronic coronary heart disease: A retrospective

297 study. ***PLoS Med*** 2021;18:1-22. doi:10.1371/journal.pmed.1003513.
298 5 Ferkingstad E, Sulem P, Atlason BA, et al. Large-scale integration of the plasma
299 proteome with genetics and disease. ***Nat Genet*** 2021;53:1712-21.
300 doi:10.1038/s41588-021-00978-w.
301 6 Sanderson E, Glymour MM, Holmes MV, et al. Mendelian randomization. ***Nat***
302 ***Rev Methods Primers*** 2022; 2, 1-21. doi:10.1038/s43586-021-00092-5.
303 7 Chen L, Peters JE, Prins B, et al. Systematic Mendelian randomization using the
304 human plasma proteome to discover potential therapeutic targets for stroke. ***Nat***
305 ***Commun*** 2022;13:1-14. doi:10.1038/s41467-022-33675-1.
306 8 Yoshiji S, Butler-Laporte G, Lu T, et al. Proteome-wide Mendelian randomization
307 implicates nephronectin as an actionable mediator of the effect of obesity on
308 COVID-19 severity. ***Nat Metab*** 2023;5:248-64. doi:10.1038/s42255-023-00742-w.
309 9 Nakanishi T, Cerani A, Forgetta V, et al. Genetically increased circulating FUT3
310 level leads to reduced risk of idiopathic pulmonary fibrosis: A Mendelian
311 randomisation study. ***Eur Respir J*** 2022;59. doi:10.1183/13993003.03979-2020.
312 10 King EA, Wade Davis J, Degner JF. Are drug targets with genetic support twice
313 as likely to be approved? Revised estimates of the impact of genetic support for drug
314 mechanisms on the probability of drug approval. ***PLoS Genet*** 2019;15:1-20.
315 doi:10.1371/journal.pgen.1008489.
316 11 Ochoa D, Karim M, Ghoussaini M, et al. Human genetics evidence supports
317 two-thirds of the 2021 FDA-approved drugs. ***Nat Rev Drug Discov*** 2022;21:551.
318 doi:10.1038/d41573-022-00120-3.
319 12 Yoshiji S, Lu TY, Butler-Laporte G, et al, COL6A3-derived endotrophin mediates
320 the effect of obesity on coronary artery disease:an integrative proteogenomics analysis.
321 ***medRxiv*** 2023. doi: 10.1101/2023.04.19.23288706.
322 13 Li SF & Gong MJ. Therapeutic targets for haemorrhoidal disease: proteome-wide
323 Mendelian randomisation and colocalization analyses. ***medRxiv*** 2023.
324 doi:10.1101/2023.06.19.23291373.
325 14 Hemani G, Zheng J, Elsworth B, et al. The MR-base platform supports systematic
326 causal inference across the human phenome. ***Elife*** 2018;7:1-29.

327 doi:10.7554/eLife.34408.
328 15 Giambartolomei C, Vukcevic D, Schadt EE, et al. Bayesian Test for
329 Colocalisation between Pairs of Genetic Association Studies Using Summary
330 Statistics. ***PLoS Genet*** 2014;10. doi:10.1371/journal.pgen.1004383.
331 16 Hong Y, Kim HJ, Park S, et al. Single Cell Analysis of Human Thyroid Reveals
332 the Transcriptional Signatures of Aging. ***Endocrinol*** (United States) 2023;164:1-12.
333 doi:10.1210/endocr/bqad029.
334 17 Carter AR, Gill D, Davies NM, et al. Understanding the consequences of
335 education inequality on cardiovascular disease: Mendelian randomisation study. ***BMJ***
336 2019;365:1-12. doi:10.1136/bmj.l1855.
337 18 Duerr RH, Taylor KD, Brant SR, et al. A genome-wide association study
338 identifies IL23R as an inflammatory bowel disease gene. ***Science*** 2006;314:1461-3.
339 doi:10.1126/science.1135245.
340 19 Burton PR, Clayton DG, Cardon LR, et al. Association scan of 14,500
341 nonsynonymous SNPs in four diseases identifies autoimmunity variants. ***Nat Genet***
342 2007;39:1329-1337. doi: 10.1038/ng.2007.17.
343 20 Kim MI. Hypothyroidism in Older Adults. [Updated 2020 Jul 14]. In: Feingold KR,
344 Anawalt B, Blackman MR, et al., editors. Endotext [Internet]. South Dartmouth (MA):
345 MDText.com, Inc.; 2000-. Available from:
346 https://www.ncbi.nlm.nih.gov/books/NBK279005/.
347 21 Zhang Y, Zhao M, Guo P, et al. Mendelian randomisation highlights
348 hypothyroidism as a causal determinant of idiopathic pulmonary fibrosis.
349 ***eBioMedicine*** 2021;73:103669. doi:10.1016/j.ebiom.2021.103669.
350 22 Allen RJ, Guillen-Guio B, Oldham JM, et al. Genome-Wide Association Study of
351 Susceptibility to Idiopathic Pulmonary Fibrosis. ***Thorax*** 2022; 77(8): 829-833. doi:
352 10.1136/thoraxjnl-2021-218577.
353

354 **Figure Legends**

355 **Figure 1 Mendelian randomisation and colocalization results.** (**A**) A diagram
356 depicting the Mendelian randomization principle and procedure filtering for MR

357 results. LOOA, leave-one-out analysis. (**B**) Shared the associations between 79
358 causative plasma proteins (related with at least one clinical trait) and 16 clinical traits
359 from MR analysis. For visualizing, only MR results showing no pleiotropy
360 (MR-Egger, *p*-value>0.5), no heterogeneity (I^2<0.5), and true causality direction
361 (Steiger test, *p*-value<0.05) were included. (**C**) The two mathematical models of
362 genetic colocalization, causation, and colocalization, as well as LD confounding. (**D**)
363 Scanning for colocalization evidence of causative plasma proteins with outcomes. The
364 size of the circle represents the posterior probability for H4, and the color of the circle
365 represents the classification of the evidence. Red indicates high evidence for
366 colocalization (PH4>0.8); yellow indicates medium evidence for colocalization
367 (PH4>0.7); and green and black indicate moderate evidence for colocalization
368 (PH4<0.7). (**E**) The locus-compare scatter plot for the CRAT, LYPLAL1, and THBS3
369 association signals. The findings of colocalization analyses for CRAT (left),
370 LYPLAL1 (center), and THBS3 (right) are shown. The marked SNP represents the
371 genetic variants used for the MR analysis.
372
373 **Figure 2 Follow-up analyses for causal proteins associated with hypothyroidism.**
374 (**A**) The locus-compare scatter plot compares the quantitative trait loci (pQTL) of
375 CA12 and the GWAS of hypothyroidism. (**B**) CA12 expression profile in human
376 tissues in GTEx v8 (https://gtexportal.org/). CA12 expression levels were displayed
377 on a log transcript per thousand plus one (TPM+1) scale. (**C**) CA12 expression
378 patterns in human thyroid tissues from thyroidectomy patients (GSE182416,
379 accessible at https://www.ncbi.nlm.nih.gov/geo/). NK cells: natural killer cells; SMCs:
380 smooth muscle cells. (**D**) A dot-plot revealing the expression of CA12 in epithelial
381 cells and fibroblasts in children and adults. (**E**) Forest plots for the effect of three
382 selected proteins on IPF. (**F**) Mediation effects of IRF3 on IPF via hypothyroidism.
383 For the effect of IRF3 on IPF mediated by hypothyroidism, the product of coefficients
384 method calculates the proportion mediated by multiplying $\beta_{\text{IRF3-to-hypothyroidism}}$ and
385 $\beta_{\text{hypothyroidism-to-IPF}}$ and subsequently dividing it by $\beta_{\text{IRF3-to-IPF}}$, where $\beta_{\text{IRF3-to-hypothyroidism}}$ is
386 the effect of IRF3 on hypothyroidism, $\beta_{\text{hypothyroidism-to-IPF}}$ is the effect of hypothyroidism

on IPF, and $\beta_{IRF3\text{-}to\text{-}IPF}$ is the total effect of IRF3 on IPF.

Supplementary Figure 1 Volcano plots depict the impact of each plasma protein on clinical traits derived from MR studies. The x-axis shows beta estimations in MR analysis, while the y-axis shows -log10(*p*-value) values from MR results. For visualizing, only MR results showing no pleiotropy (MR-Egger, *p*-value>0.5), no heterogeneity (I^2<0.5), and true causality direction (Steiger test, *p*-value<0.05) were included.

Supplementary Tables1 The summary statistics obtained in this study.

Fig 1

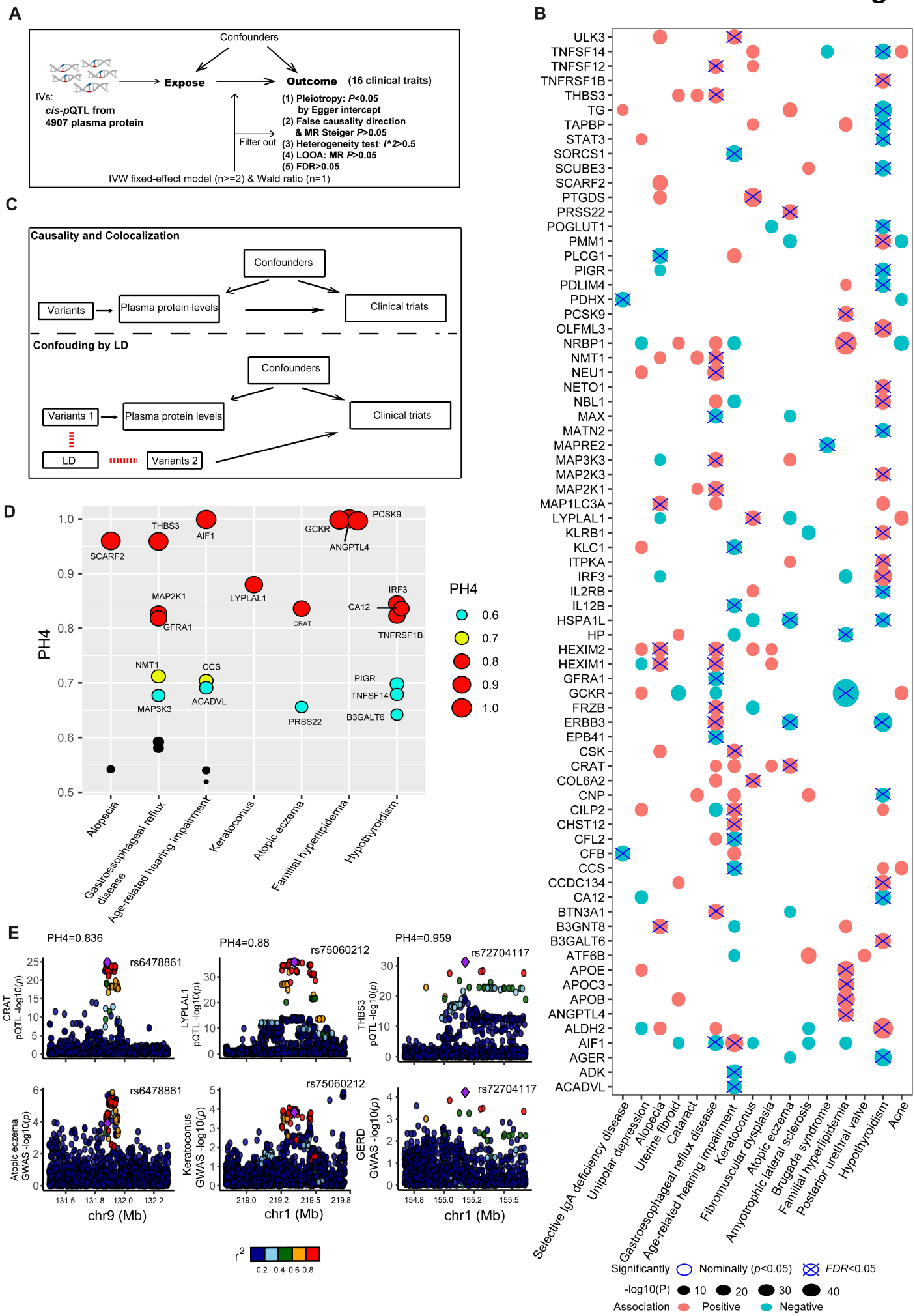
A
Confounders
Expose
Outcome (16 clinical traits)
IVs:
cis-pQTL from
4907 plasma protein
(1) Pleiotropy: P<0.05
by Egger intercept
(2) False causality direction
& MR Steiger P>0.05
Filter out
(3) Heterogeneity test: I^2>0.5
(4) LOOA: MR P>0.05
(5) FDR>0.05
IVW fixed-effect model (n>=2) & Wald ratio (n=1)
B
ULK3
TNFSF14
TNFSF12
TNFRSF1B
THBS3
TG
TAPBP
STAT3
SORCS1
SCUBE3
SCARF2
PTGDS
PRSS22
POGLUT1
PMM1
PLCG1
PIGR
PDLIM4
PDHX
PCSK9
OLFML3
NRBP1
NMT1
NEU1
NETO1
NBL1
MAX
MATN2
MAPRE2
MAP3K3
MAP2K3
MAP2K1
MAP1LC3A
LYPLAL1
KLRB1
KLC1
ITPKA
IRF3
IL2RB
IL12B
HSPA1L
HP
HEXIM2
HEXIM1
GFRA1
GCKR
FRZB
ERBB3
EPB41
CSK
CRAT
COL6A2
CNP
CILP2
CHST12
CFL2
CFB
CCS
CCDC134
CA12
BTN3A1
B3GNT8
B3GALT6
ATF6B
APOE
APOC3
APOB
ANGPTL4
ALDH2
AIF1
AGER
ADK
ACADVL
Selective IgA deficiency disease
Unipolar depression
Alopecia
Uterine fibroid
Cataract
Gastroesophageal reflux disease
Age-related hearing impairment
Keratoconus
Atopic eczema
Fibromuscular dysplasia
Amyotrophic lateral sclerosis
Brugada syndrome
Familial hyperlipidemia
Posterior urethral valve
Hypothyroidism
Acne
Significantly
Nominally (p<0.05)
FDR<0.05
-log10(P)
10
20
30
40
Association
Positive
Negative
C
Causality and Colocalization
Confounders
Variants
Plasma protein levels
Clinical triats
Confouding by LD
Confounders
Variants 1
Plasma protein levels
Clinical triats
LD
Variants 2
D
PH4
1.0
0.9
0.8
0.7
0.6
0.5
SCARF2
THBS3
AIF1
GCKR
PCSK9
ANGPTL4
MAP2K1
GFRA1
LYPLAL1
CRAT
CA12
IRF3
TNFRSF1B
NMT1
MAP3K3
CCS
ACADVL
PRSS22
PIGR
TNFSF14
B3GALT6
PH4
0.6
0.7
0.8
0.9
1.0
Alopecia
Gastroesophageal reflux disease
Age-related hearing impairment
Keratoconus
Atopic eczema
Familial hyperlipidemia
Hypothyroidism
E
PH4=0.836
rs6478861
CRAT pQTL -log10(p)
PH4=0.88
rs75060212
LYPLAL1 pQTL -log10(p)
PH4=0.959
rs72704117
THBS3 pQTL -log10(p)
rs6478861
Atopic eczema GWAS -log10(p)
chr9 (Mb)
rs75060212
Keratoconus GWAS -log10(p)
chr1 (Mb)
rs72704117
GERD GWAS -log10(p)
chr1 (Mb)
r2
0.2
0.4
0.6
0.8

Fig 2

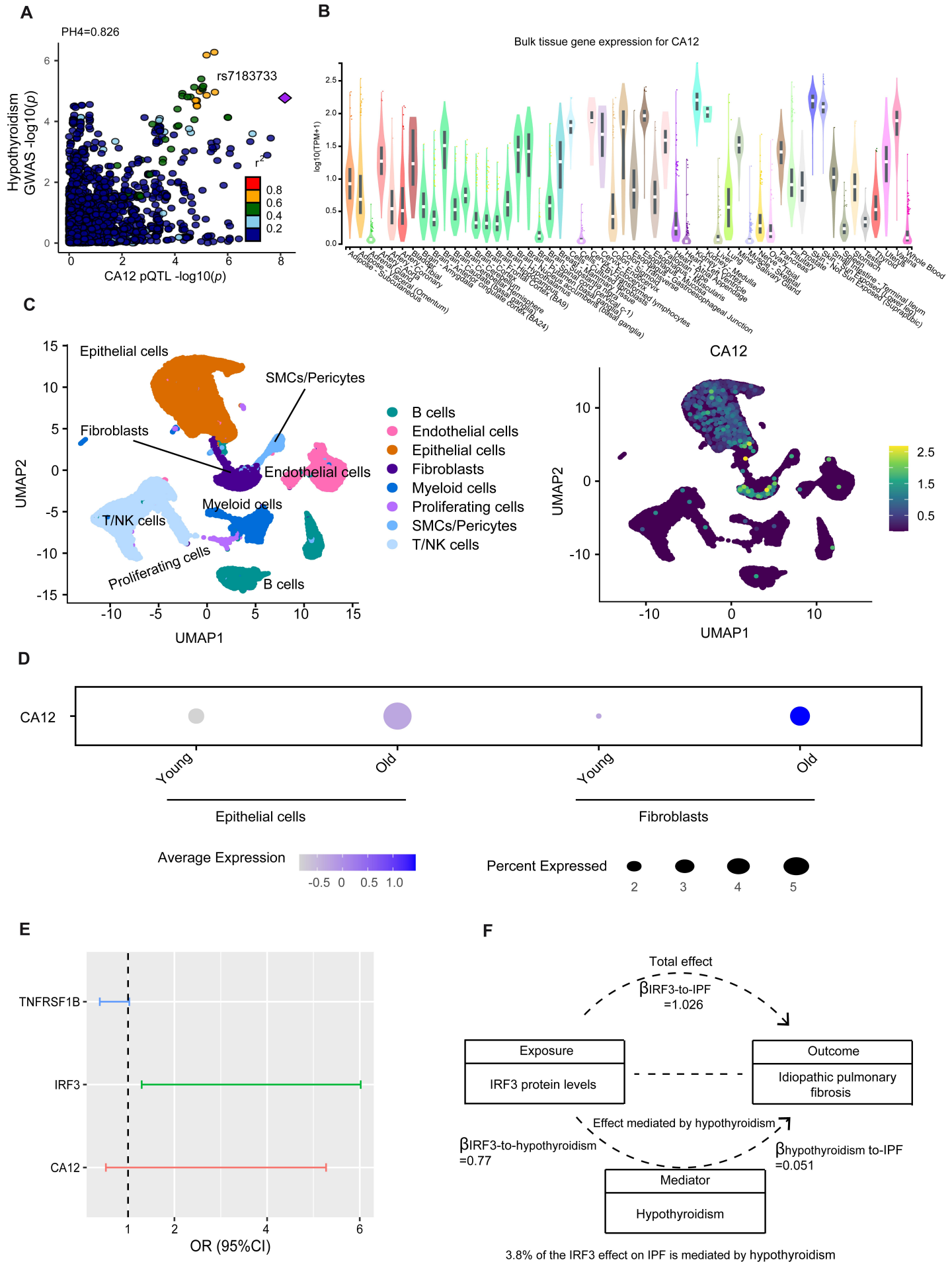
A
PH4=0.826
rs7183733
Hypothyroidism GWAS -log10(p)
CA12 pQTL -log10(p)
r²
0.8
0.6
0.4
0.2
B
Bulk tissue gene expression for CA12
log10(TPM+1)
CA12
C
Epithelial cells
SMCs/Pericytes
Fibroblasts
Endothelial cells
Myeloid cells
T/NK cells
Proliferating cells
B cells
UMAP1
UMAP2
D
CA12
Young
Old
Epithelial cells
Fibroblasts
Average Expression
Percent Expressed
E
TNFRSF1B
IRF3
CA12
OR (95%CI)
F
Total effect
βIRF3-to-IPF =1.026
Exposure
IRF3 protein levels
Outcome
Idiopathic pulmonary fibrosis
Effect mediated by hypothyroidism
βIRF3-to-hypothyroidism =0.77
βhypothyroidism to-IPF =0.051
Mediator
Hypothyroidism
3.8% of the IRF3 effect on IPF is mediated by hypothyroidism

Fig S1

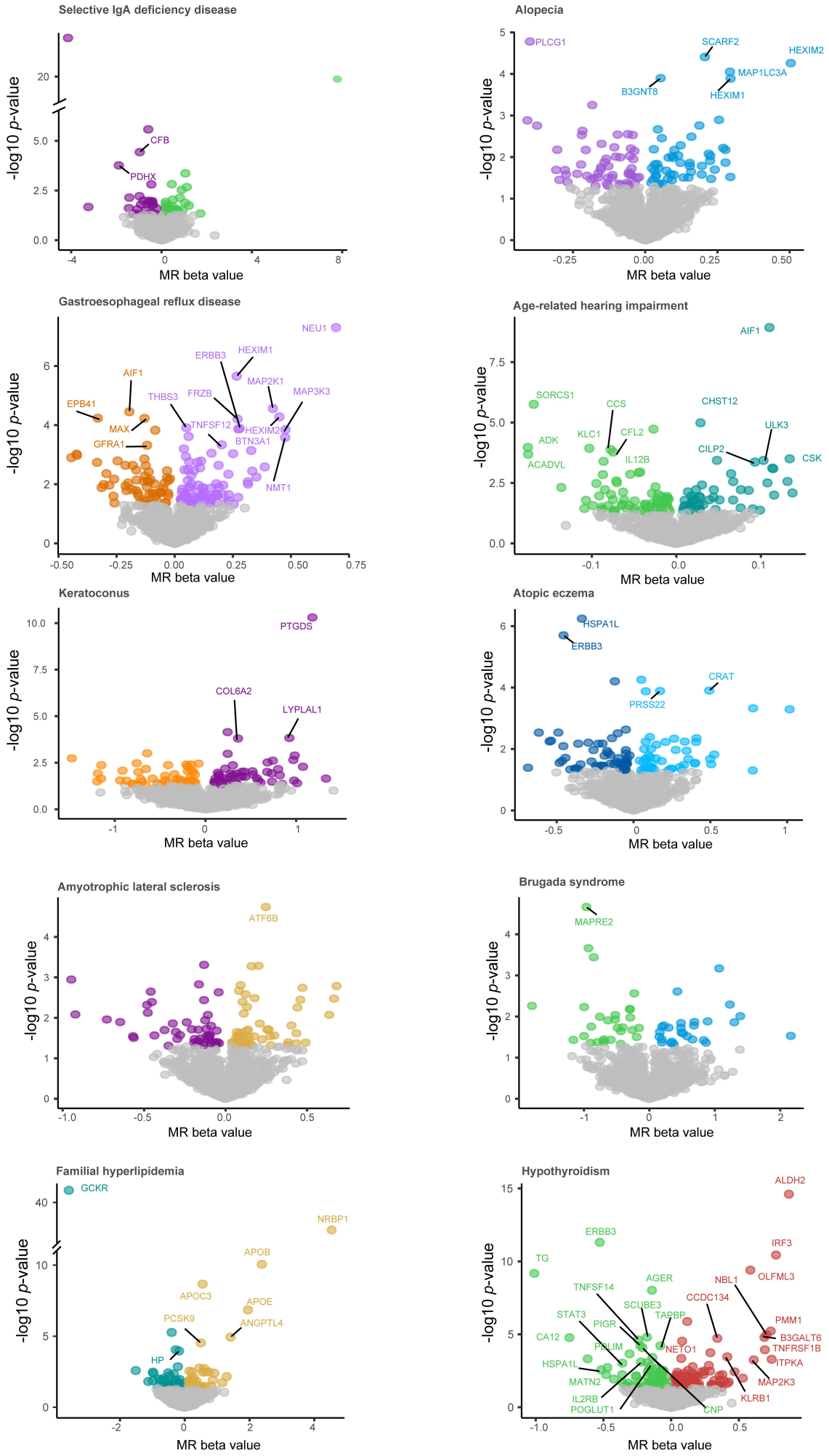
Selective IgA deficiency disease
-log10 p-value
MR beta value
CFB
PDHX
Alopecia
PLCG1
SCARF2
HEXIM2
MAP1LC3A
B3GNT8
HEXIM1
Gastroesophageal reflux disease
NEU1
ERBB3
HEXIM1
AIF1
MAP2K1
MAP3K3
THBS3
FRZB
EPB41
MAX
TNFSF12
HEXIM2
GFRA1
BTN3A1
NMT1
Age-related hearing impairment
AIF1
SORCS1
CCS
CHST12
ULK3
ADK
KLC1
CFL2
CILP2
CSK
ACADVL
IL12B
Keratoconus
PTGDS
COL6A2
LYPLAL1
Atopic eczema
HSPA1L
ERBB3
CRAT
PRSS22
Amyotrophic lateral sclerosis
ATF6B
Brugada syndrome
MAPRE2
Familial hyperlipidemia
GCKR
NRBP1
APOB
APOC3
APOE
PCSK9
ANGPTL4
HP
Hypothyroidism
ALDH2
ERBB3
IRF3
TG
OLFML3
AGER
NBL1
TNFSF14
CCDC134
SCUBE3
STAT3
TARBP
PMM1
PIGR
B3GALT6
CA12
PDLIM
NETO1
TNFRSF1B
ITPKA
HSPA1L
MAP2K3
MATN2
KLRB1
IL2RB
POGLUT1
CNP